




Cell-specific targeting of extracellular vesicles through engineering the glycocalyx

Wenyi Zheng^{1,2}  | Rui He^{2,3} | Xiuming Liang^{1,2}  | Samantha Roudi^{1,2} |
 Jeremy Bost^{1,2} | Pierre-Michael Coly^{4,5} | Guillaume van Niel^{4,5}  |
 Samir E. L. Andaloussi^{1,2,6}

¹Biomolecular Medicine, Division of Biomolecular and Cellular Medicine, Department of Laboratory Medicine, Karolinska Institutet, Huddinge, Sweden

²Centre for Allogeneic Stem Cell Transplantation (CAST), Karolinska University Hospital, Huddinge, Sweden

³Experimental Cancer Medicine, Division of Biomolecular and Cellular Medicine, Department of Laboratory Medicine, Karolinska Institutet, Huddinge, Sweden

⁴Université de Paris, Institute of Psychiatry and Neuroscience of Paris (IPNP), INSERM U1266, Paris, France

⁵GHU Paris Psychiatrie et Neurosciences, Hôpital Sainte Anne, Paris, France

⁶EVOX Therapeutics Limited, Oxford, UK

Correspondence

Wenyi Zheng, Biomolecular Medicine, Division of Biomolecular and Cellular Medicine, Department of Laboratory Medicine, Karolinska Institutet, Huddinge, Sweden.

Email: wenyi.zheng@ki.se; samir.el-andaloussi@ki.se

Funding information

H2020 European Research Council, Grant/Award Numbers: 101001374, 825828; EVOX Therapeutics Ltd; Stiftelsen för Strategisk Forskning, Grant/Award Number: IRC15-0065; Institut National Du Cancer, Grant/Award Number: INCA N°2019-125 PLBIO19-059; Medicinska Forskningsrådet, Grant/Award Number: 2020-01322; ANR ZENITH, Grant/Award Number: ANR-20-CE18-0026_01

Abstract

Extracellular vesicles (EVs) are promising carriers for the delivery of a variety of chemical and biological drugs. However, their efficacy is limited by the lack of cellular specificity. Available methods to improve the tissue specificity of EVs predominantly rely on surface display of proteins and peptides, largely overlooking the dense glycocalyx that constitutes the outermost layer of EVs. In the present study, we report a reconfigurable glycoengineering strategy that can endogenously display glycans of interest on EV surface. Briefly, EV producer cells are genetically engineered to co-express a glycosylation domain (GD) inserted into the large extracellular loop of CD63 (a well-studied EV scaffold protein) and fucosyltransferase VII (FUT7) or IX (FUT9), so that the engineered EVs display the glycan of interest. Through this strategy, we showcase surface display of two types of glycan ligands, sialyl Lewis X (sLeX) and Lewis X, on EVs and achieve high specificity towards activated endothelial cells and dendritic cells, respectively. Moreover, the endothelial cell-targeting properties of sLeX-EVs were combined with the intrinsic therapeutic effects of mesenchymal stem cells (MSCs), leading to enhanced attenuation of endothelial damage. In summary, this study presents a reconfigurable glycoengineering strategy to produce EVs with strong cellular specificity and highlights the glycocalyx as an exploitable trait for engineering EVs.

KEYWORDS

CD15, CD15s, CD209, endothelium, exosomes, extracellular vesicles, lectin

1 | INTRODUCTION

Extracellular vesicles (EVs) are lipid bilayer-enclosed particles secreted by all cells (Kalluri & LeBleu, 2020). The membranous structures are capable of shielding luminal environment-sensitive nucleic acids and displaying functional ligands amid juxtacrine

This is an open access article under the terms of the [Creative Commons Attribution-NonCommercial-NoDerivs License](https://creativecommons.org/licenses/by-nc-nd/4.0/), which permits use and distribution in any medium, provided the original work is properly cited, the use is non-commercial and no modifications or adaptations are made.

© 2022 The Authors. *Journal of Extracellular Vesicles* published by Wiley Periodicals, LLC on behalf of the International Society for Extracellular Vesicles.

signalling (Wiklander et al., 2019). These prominent properties are inspiring the development of EV-based therapy. Native EVs derived from cells with proven clinical benefits like mesenchymal stem cells (MSCs), chimeric antigen receptor-T cells, and natural killer cells have been reported to carry functional cargo molecules and exert therapeutic effects on their own (Fu et al., 2019; Johnson et al., 2021; Panda et al., 2021; Wu et al., 2019). An alternative avenue to generate therapeutic vesicles lies in EV engineering using various endogenous and exogenous approaches (Kwon et al., 2021; Y. Liang et al., 2021; Richter et al., 2021; Teng & Fussenegger, 2021).

Despite advances to produce EVs in a customized manner, a general hurdle facing EV-based therapy is the relatively low specificity to target cells. As such, EV surface has been extensively tailored to display functional moieties that are recognized by target cells (Richter et al., 2021). This is commonly achievable through genetic engineering of EV producer cells to express a fusion protein consisting of the moiety of interest and an EV-sorting membrane protein such as Lamp2b or PTGFRN (Alvarez-Erviti et al., 2011; Dooley et al., 2021). Alternatively, targeting moieties are incorporated into pre-isolated EVs through chemical reactions at bio-orthogonal conditions or non-covalent association. For instance, the synthetic peptide CP05 was identified as a strong binder for the EV surface protein CD63 and coupling CP05 to targeting ligands generated exogenously labelled EVs that were successfully deployed for cellular targeting (Gao et al., 2018; Wang et al., 2022).

Until now, almost all strategies for EV surface display focus on the use of protein and peptide ligands, while the dense glycocalyx coating that forms the outermost layer of EVs is largely overlooked (Gerlach & Griffin, 2016). Indeed, rational glycoengineering has shown promises to enhance the therapeutic efficacy of adoptive cell therapies. For instance, natural killer cells displaying the glycan ligand of CD22 had higher affinity and activity against leukemic B cells than non-targeted cells (Hong et al., 2020). In terms of glycoengineering of EVs, two earlier studies trimmed surface glycans using enzymatic digestion and found significant changes in cellular uptake and biodistribution profiles, highlighting the functional relevance of surface glycans (Royo et al., 2019; Williams et al., 2019). However, enzymatic deglycosylation is limited by the flexibility required for manipulating a designated glycan to enable cellular targeting.

Sialyl Lewis-X (sLeX) is a tetrasaccharide glycan ligand of E-selectin (Stahn et al., 1998). It is expressed by leukocytes and implicated in leukocyte adhesion to E-selectin-expressing endothelial cells during inflammation (Henseleit et al., 1996). The ability of sLeX to target activated endothelial cells has been leveraged to improve the accumulation of synthetic nanoparticles like liposomes and microbubbles towards inflammatory lesions (Jubeli et al., 2012). In those studies, sLeX was exogenously associated onto particle surface and further removal of unconjugated glycan through purification was required, which might be problematic for large-scale production. In contrast, by genetically engineering EV producer cells, the targeting ligands are endogenously sorted onto EVs and no purification procedure is required (Jia et al., 2021). In this study, we use a genetic engineering approach to display sLeX on the surface of EVs and characterize their ability to target activated endothelial cells. Moreover, the adaptability of the strategy is examined through surface display of another glycan ligand, LeX, for targeting DC-SIGN-expressing dendritic cells. Our results show that engineering the glycan profile of EVs is a viable strategy for tailoring their cellular specificity.

2 | MATERIALS AND METHOD

2.1 | Cloning

All transgenes were codon-optimized and ordered from IDT (Integrated DNA Technologies). They were cloned downstream of the CAG promoter into the pLEX vector and transferred to lentiviral vectors using restriction enzymes. All expression cassettes were confirmed by SANGER sequencing. Plasmids are available from the corresponding author upon request.

2.2 | Cell culture

B16F10 cells, HEK-293T cells and their derived stable cells were maintained in high glucose DMEM media (Gibco, 41966-029) supplemented with 10% fetal bovine serum (FBS; Gibco, 10270-106) and 1% anti-anti (Gibco, 15240). HUVEC and HAEC were cultured in Endothelial Cell Growth Medium MV 2 (PromoCell, C-22022) supplemented with 1% anti-anti. Human cord blood-derived MSCs, MSC-derived stable cells and cEND were cultured in MEM media (Gibco, 22561-021) supplemented with 10% FBS and 1% anti-anti. Freestyle 293-F cells and the derived stable cells were kept in FreeStyle 293 Expression Media (Gibco, 12338-018) under continuous shaking at 175 RPM. All cells were cultured in humidified incubators with 37°C and 5% CO₂.

2.3 | Lentiviral production

HEK-293T cells were seeded in T175 flasks and cultured until cell confluency was around 60%. The cells were co-transfected with the lentiviral vectors encoding transgenes, pCD/NL-BH (helper plasmid) and pcoPE01(envelope plasmid) overnight and

then cultured in complete DMEM supplemented with 10 mM sodium butyrate (Sigma-Aldrich, B5878) for 6 h. The media were changed to complete DMEM medium and kept for 22 h. To pellet viral particles, the conditioned media were passed through 0.45 μm syringe filters and centrifuged at 25,000 g for 90 min at 4°C. The pellets were resuspended with freshly prepared medium (IMDM with 20% FBS) and stored at -80°C until use.

2.4 | Generation of stable cell lines

HEK-293T and MSCs were seeded in six-well plates and incubated until the confluency reaching around 60%. The cells were transduced with lentiviral particles overnight and passaged to T75 flasks for expansion. For FreeStyle 293-F, cells were seeded in Erlenmeyer flasks (Sigma-Aldrich, CLS431143) at 2.5×10^5 /ml and cultured overnight before lentiviral transduction. Engineered cells were selected using puromycin (4 $\mu\text{g}/\text{ml}$; Sigma-Aldrich, P8833) and/or blasticidin (20 $\mu\text{g}/\text{ml}$; Sigma-Aldrich, 203350). A total of 26 types of stable cell lines were established as listed in Table S1.

2.5 | Isolation of EVs

Conditioned media were pre-cleared by two rounds of centrifugation (700 g for 5 min and then 2000 g for 10 min) and filtration (200 nm) to sequentially deplete cells, cellular debris and large particles. The media were concentrated and diafiltrated to roughly 50 ml using the KrosFlo KR2i TFF System (Repligen, US) with 300 kDa cut-off hollow fibre filters (Spetrum Labs, D06-E300-05-N) at a flow rate of 100 ml/min and transmembrane pressure of 3.0 psi. EVs were further concentrated till around 500 μl using spin-filter with 10 kDa molecular weight cut-off (Amicon Ultra-15; Millipore, UFC910024) and stored in human albumin-trehalose (HAT) buffer at -80°C until use (Görgens et al., 2022).

2.6 | Size exclusion chromatography

500 μl of EVs (1×10^{11} /ml) were loaded onto size exclusion columns (Izon, SP1). According to the manufacturer's instruction, the first 3 ml of the eluate were void volume and discarded. Then, a total of 48 fractions (300 μl per fraction) were collected and numbered as 1–48. Fractions 1–10 and fractions 11–48 were enriched with EVs and free proteins, respectively.

2.7 | Western blotting

EVs (5×10^9 in 15 μl) were mixed with 5 μl of sample buffer (ThermoFisher, NP0007). After heating at 70°C for 10 min, the mixture was loaded onto a NuPAGE Novex 4%–12% Bis-Tris Protein Gel (Invitrogen, NP0335BOX) and separated at 120 V in NuPAGE MES SDS running buffer (Invitrogen, NP0002) for 2 h. Proteins on the gel were transferred to a nitrocellulose membrane (Invitrogen, IB23001) at 20 V for 7 min using the iBlot system. Membranes were immersed in blocking buffer (LI-COR, 927–60004) at room temperature for 1 h under gentle shaking and incubated with primary antibody overnight at 4°C. Membranes were rinsed with Tris-buffered saline supplemented with 0.1% Tween 20 (TBS-T) for three times over 15 min and stained with corresponding secondary antibodies (1: 5,000 for all, LI-COR) for 1 h. After rinsing with TBS-T for three times over 15 min and TBS once, membranes were imaged using Odyssey infrared imaging system (LI-COR, US). The following primary antibodies were used: anti-Nluc (Promega, 9PIN7000; 1:1000) and sLeX (BD, 551344; 1:500).

2.8 | Nanoparticle tracking analysis

Nanoparticle tracking analysis (NTA; NanoSight NS500, Malvern Panalytic, UK) was used to measure particle size and concentration. EVs were diluted in 200 nm-filtered PBS and five videos (30-sec each) were acquired for each sample with a camera level of 13. Data were analyzed using NTA 3.2 software with screen gain and minimum track length of 20 and 3, respectively.

2.9 | Binding to recombinant receptors

Protein A-functionalized plates (ThermoFisher, 15132) were rinsed with dilution buffer (0.1% BSA in PBS) and coated with 100 μl of Fc-tagged recombinant receptors (2 $\mu\text{g}/\text{ml}$ in dilution buffer) for 1 h. The plates were rinsed twice to remove unbound receptors and incubated with 100 μl of EVs (1×10^8 /ml) for 2 h. After removal of unbound EVs, 100 μl of Triton X-100 solution (0.1% in PBS)

was added to lyse bound EVs. Three types of recombinant receptors were used: mouse E-selectin (BioLegend, 755504), mouse P-selectin (BioLegend, 755402) and human DC-SIGN (R&D systems, 161-DC-050).

2.10 | Cryo-electron microscopy

Holey carbon-coated grid (Quantifoil, Germany) was glow-discharged for better absorbing EVs. Extra liquid on the grid was removed using filter paper. The grid was subsequently vitrified into liquid ethane at -178°C using a Vitrobot (FEI, Netherlands) and transferred onto a Philips CM200-FEG electron microscope (FEI, Netherlands) using a Gatan 626 cryo-holder (GATAN Inc, USA). Electron images were acquired using an accelerating voltage of 200 kV and nominal magnification of 50,000. Defocus values ranged from $-2\ \mu\text{m}$ to $-3\ \mu\text{m}$. Micrographs were recorded using a CMOS camera (TVIPS, Germany) at $4\text{K} \times 4\text{K}$.

2.11 | Confocal microscopy

HUVEC cells were seeded at 5×10^4 per well in 24-well glass-bottom chamber slides (ThermoFisher; 155409) and incubated overnight. The cells were stimulated with TNF- α (20 ng/mL) for 2 h, rinsed, and treated with mNG-labeled EVs (2×10^9 /mL) for another 2 h. Hoechst 33342 (ThermoFisher, R37605) and LysoTracker Red DND 99 (ThermoFisher, L7528) were added to counterstain the nuclei and lysosome, respectively. The chamber slides were transferred to a microscope stage-top incubator at 37°C with 5% CO_2 . Images were acquired using a confocal microscope (A1R confocal, Nikon, Japan) and analyzed by the NIS-Elements software (Nikon, Japan). 3D reconstruction was compiled with a height of $10\ \mu\text{m}$ and a resolution of $0.3\ \mu\text{m}$.

2.12 | Cellular uptake

Endothelial cells were seeded at 5×10^4 per well in 24-well plates and incubated overnight. The cells were stimulated with TNF- α (20 ng/ml) or lipid polysaccharide (5 ng/ml) for 2 h, rinsed, and treated with 2×10^9 /mL EVs for another 4 h if not otherwise specified. The uptake of Nluc-labelled and mNG-labelled EVs was assessed by quantification of cellular Nluc after cell lysis and fluorescence intensity after trypsinization, respectively. In certain conditions, TNF- α -activated endothelial cells were co-treated with antibodies against human E-selectin (BD, 551144; $5\ \mu\text{l}$ per well) or sLeX (BD, 563526; $3\ \mu\text{l}$ per well) and EVs.

2.13 | Magnetic-activated cell sorting

After cleaning faeces, the colon was cut longitudinally and then laterally into pieces of approximately 0.5 cm in length. Single cells were prepared following the Lamina Propria Kit instructions (Miltenyi, 130-097-410). Endothelial cells were positively selected using CD31 microbeads (Miltenyi, 130-097-418) and LS columns (Miltenyi, 130-042-401). Both CD31-positive and -negative fractions were collected and total proteins were quantified using the BCA protein assay (ThermoFisher, 23225).

2.14 | Flow cytometry for cells

For characterization of endothelial cell lines, colon cells and mouse bone marrow-derived dendritic cells (mBMDCs), the cells were first stained with appropriate antibodies and resuspended in $100\ \mu\text{l}$ of PBS containing 2% FBS before analysis. DAPI (4',6-diamidino-2-phenylindole) was added to all cell samples to exclude dead cells from the analysis. The samples were measured using MACSQuant Analyzer 10 cytometer (Miltenyi, Germany). Data were analyzed with FlowJo software (version 10.6.2) and doublets were excluded by forward scatter area versus height gating.

To simultaneously detect glycans and EVs using MACSQuant Analyzer 10 cytometer, EVs were firstly pulled down using magnetic beads coated with CD63 (ThermoFisher, 10606D) and CD81 (ThermoFisher, 10622D) antibodies following the manufacturer's instructions. The bead-EV complexes were rinsed and stained with antibodies against sLeX or LeX for 1 h at room temperature before analysis.

2.15 | Flow cytometry for EVs

Amnis® CellStream instrument (Luminex, US) was used to detect EVs at single-vesicle level. EVs without fluorescent tags were first stained with $0.4\ \mu\text{l}$ of sLeX antibodies (diluted by 10-fold) overnight. The stained and mNG-labelled EVs were analyzed using the side scatter laser (SSC; 40% of maximum power), 488 nm laser (maximum power) and 642 nm laser (maximum power). All

data were acquired at a flow rate of 3.44 $\mu\text{l}/\text{min}$. SSC and AF647 signals were collected in channel 1 (773 ± 56 nm filter) and channel B6 (702 ± 87 nm filter), respectively. AF488 and mNG signals were collected in channel C3 (528 ± 46 nm filter). DPBS (Gibco, 14190-136) was used as sheath fluid without further filtration. Data were analyzed with optimized masking settings using the FlowJo software.

The following antibodies and corresponding isotypes were used: sLeX-AF488 (BD, 563528), sLeX-AF647 (BD, 563526), LeX-APC (BD, 561716), CD11c-PE (BD, 557401), F4/80-BV510 (BD, 743280), DC-SIGN-PE (BioLegend, 833004), and E-selectin-APC (BD, 551144).

2.16 | Colitis mouse model

All procedures were performed in accordance with ethical permission granted by Swedish Jordbruksverket (No. 16212-2020). Female Balb/c mice of around 20 g were anaesthetized with isoflurane and instilled with 100 μl of 2% picrylsulfonic acid (Sigma-Aldrich, P2297) into the rectum. The next day, 100 μl of Nluc-labeled EVs ($5e^{10}$ particles per mouse) were injected through the tail vein. After 30 min, mice were bled for collecting blood in EDTA-coated tubes and sacrificed for collecting colon and major organs. Blood samples were immediately centrifuged at 2000 g for 10 min to retrieve plasma. The organs were weighed and lysed in 1 ml of Triton X-100 solution using a TissueLyser II (QIAGEN, Germany). To isolate endothelial cells in the colon, the colon was dissected and immediately placed in ice-cold HBSS (Gibco, 14175129).

2.17 | B16F10 mouse model

All procedures were performed in accordance with ethical permission granted by Swedish Jordbruksverket (No. 2173-2021). C57BL/6J mice with a body weight of around 20 g were anesthetized with isoflurane and subcutaneously inoculated with 100 μl of B16F10 cells ($5e^5$ cells per mouse) at the right dorsal. At around 14 days post inoculation, tumour sizes reached around 0.5 cm^3 . 100 μl of Nluc-labelled EVs ($5e^{10}$ particles per mouse) were injected through the tail vein. Blood, tumour and major organs were collected 30 min later for the analysis of Nluc.

2.18 | Detection of luciferase using luminometer

Nluc was quantified in six types of samples: EVs, SEC eluate, plate-bound EVs, cell lysate, mouse plasma and tissue lysate. To measure Nluc in EVs, 5 μl of EVs were added into white-walled 96-well plates along with 20 μl of Triton X-100 solution. The plate was shaken horizontally at 500 rpm for 5 min. For plate-bound EVs and cell lysate, 25 μl of the lysate were added to the plate. For SEC eluate, 25 μl of samples were lysed with equal volume of Triton-X solution. For mouse plasma, 5 μl of plasma was lysed with 20 μl Triton X-100 solution. Tissue lysate was first diluted by 10-fold and 25 μl of the diluted samples were added. GloMax 96 Microplate Luminometer (Promega, US) was used to automatically inject the substrate Nano-Glo (Promega; N1130) at 25 μl per well and measure luminescence intensity.

To detect HiBiT in EVs, 10 μl of samples was added into white-walled 96-well plates and lysed with 10 μl Triton X-100 solution. Then, 20 μl of HiBiT Lytic Detection mixture (Promega; N3040) was added to each well. After incubation at room temperature under horizontal shaking at 500 RPM for 10 min, the plate was immediately measured.

2.19 | Statistics

Data are shown as mean \pm standard deviation of biological replicates and analyzed using two-tailed unpaired *t*-test. n.s.: non-significant; **p* < 0.05; ***p* < 0.01; ****p* < 0.001.

3 | RESULTS

3.1 | Combination of fucosyltransferase and glycosylation domain improves surface display of sLeX on EVs

Protein glycosylation occurs at specific residues and is carried out by a series of glycotransferase. Fucosyltransferase VII (FUT7) catalyzes the transfer of L-fucose to the N-acetylglucosamine (GlcNAc) of a distal alpha 2,3 sialylated lactosamine unit and participates in the final biosynthesis of sLeX (Lowe, 2002; Schneider et al., 2017). In a previous study, exogenous expression of FUT7 was found to increase surface display of sLeX on HEK-293T cells by 2.6-fold in comparison to wild-type counterparts, whilst expression of the sLeX protein carrier PSGL-1 alone did not lead to any significant increase (Buffone et al., 2013). Interestingly,

co-expression of FUT7 and PSGL-1 enhanced surface display of sLeX on cells by 13.9-fold, suggesting that both the fucosyltransferase and the sLeX protein carrier are required for optimal expression of sLeX.

To enrich sLeX expression on EV surface, we sought to convert CD63, a well-studied scaffold protein for genetic engineering of EVs, into a novel sLeX protein carrier. Given its distinct topology as a multi-pass membrane protein, the large extracellular loop of CD63 has been genetically engineered for surface display of functional moieties like albumin-binding domain (56-mer peptide) (X. Liang et al., 2022). Since reported sLeX protein carriers usually consist of several hundreds of amino acids and direct fusion of them into CD63 might compromise the stability and EV-sorting ability of the fusion protein, we prioritized short glycosylation domains (GDs) over full-length proteins. Following this notion, we searched the literature and found that P19 (19-mer, derived from PSGL-1) and CTP (28-mer, from beta-chorionic gonadotropin) were potential sLeX peptide carriers (Ceaglio et al., 2016; Liao et al., 2016; Stahn et al., 2005). The two peptides have one and four predicted residues for O-glycosylation, the predominant sLeX distribution pattern (Table S2), respectively, and were cloned into the large extracellular loop of CD63. To facilitate quantification of engineered EVs, a luciferase reporter Nluc was fused to the C-terminal of CD63 (Gupta et al., 2020), forming a novel sLeX protein carrier CD63-GD-Nluc (Figure 1a).

HEK-293T cells, the model EV producer cells, were transduced with lentiviral vectors encoding FUT7 and/or CD63-GD-Nluc, resulting in seven stable cell lines (Table S1). The expression level of sLeX on cells and EVs was quantified by flow cytometry after immunostaining with AF488-tagged antibodies (Figures S1a and 1b). In line with the previous study, co-expressing FUT7 and CD63-P19-Nluc (abbreviated as F7CPN) or CD63-CTP-Nluc (F7CCN) enhanced the surface display of sLeX on cells in comparison to either alone (Figure S1b and Table S1). Notably, expression of both FUT7 and CD63-GD-Nluc led to significant increases in the concentration of sLeX-EVs and density of sLeX per vesicle (Figure 1c).

The increased yield of sLeX-EVs is likely driven by enhanced production of EVs in general, transduction efficiency or glycosylation efficiency, or a combination of any of the three (Figure 1d). To elucidate the underlying mechanism(s), we normalized the concentration of sLeX-EVs against that of the whole vesicles and Nluc activity to adjust for EV production and transduction efficiency, respectively. Compared to the groups without FUT7 and/or GD, F7CPN and F7CCN retained significantly higher yield of sLeX-EVs (Figure 1e), indicating that neither general EV production nor transduction efficiency was playing a major role. To detect the extent of glycosylation, we blotted sLeX antigens in EV lysates. CN did not express sLeX, whereas F7CPN and F7CCN had detectable sLeX bands corresponding to the CD63-GD-Nluc fusion proteins (Figure S1c).

Furthermore, we replaced Nluc with the fluorescent protein mNeonGreen (mNG) to detect sLeX at a single-vesicle level. A total of four types of stable cell lines expressing mNG were established from HEK-293T cells (Figure S1d) and EVs thereof were analyzed after counter-staining with AF647-tagged sLeX antibodies (Figure 1f). The results corroborate that it was the higher glycosylation efficiency that contributed to higher yield of sLeX-EVs when combining FUT7 and either of the two GDs (Figure 1g). For F7CPN and F7CCN, the percentage of sLeX-positive EVs among mNG-labeled EVs was around 50% which could be increased while using higher sLeX antibody titer ($\geq 83\%$; Figure S1e). We additionally tested the robustness of the glyco-engineering strategy using transient transfection (Figure S2). In line with the findings from the viral transduction experiments, combination of FUT7 and GD improved the yield of sLeX-EVs in spite of the observation that FUT7 alone was adequate to drive sLeX expression on cells and EVs. Collectively, the results substantiate our glycoengineering strategy for robust surface display of sLeX on EVs.

3.2 | Glycoengineered EVs exhibit typical vesicular features and strong binding to E-selectin

With the high efficiency in surface display of sLeX, we continued to characterize the physicochemical and functional properties of sLeX-EVs. Similar to non-targeting EVs, sLeX-EVs, irrespective of the GD or reporter, had diameters of around 110 nm (Figure 2a). Morphological characterization using cryo-electron microscopy confirmed the presence of circular membranous structures (Figures 2b and S3). To simultaneously detect sLeX and EV markers, EVs were pulled down using magnetic beads coated with antibodies against CD63 or CD81 (Figure 2c). As expected, we did not observe sLeX expression on non-targeting EVs, while F7CPN and F7CCN were highly positive for sLeX (Figure 2c). The same trend was observed for mNG-labelled EVs (Figure S4a), aligning with the results above that our glycoengineering strategy applies to different reporter protein.

To validate the functional relevance of sLeX, we intended to use Nluc activity as a surrogate readout. The presence of free Nluc proteins in the EV preparations was first assessed via examining their elution profiles on size exclusion chromatography columns. For all types of EVs that were routinely concentrated using tangential flow filtration and spin-filtration, we only observed a single peak in the typical EV elution fractions corresponding to engineered EVs (Figure 2d).

Moving forward, we evaluated the binding of sLeX-EVs to recombinant E-selectin receptors. Notably, F7CPN and F7CCN were strongly bound to the plates coated with E-selectin, corresponding to a more than 240-fold enhancement compared to vehicle-coated plates; however, non-targeting EVs did not show any binding (Figure 2e). Since P-selectin is also reported to recognize sLeX-carrying PSGL-1, we measured the binding of sLeX-EVs to recombinant P-selectin (Figure S4b). F7CPN and F7CCN did bind to P-selectin but with much lower efficiency (less than 12-fold enhancement) in relation to E-selectin.

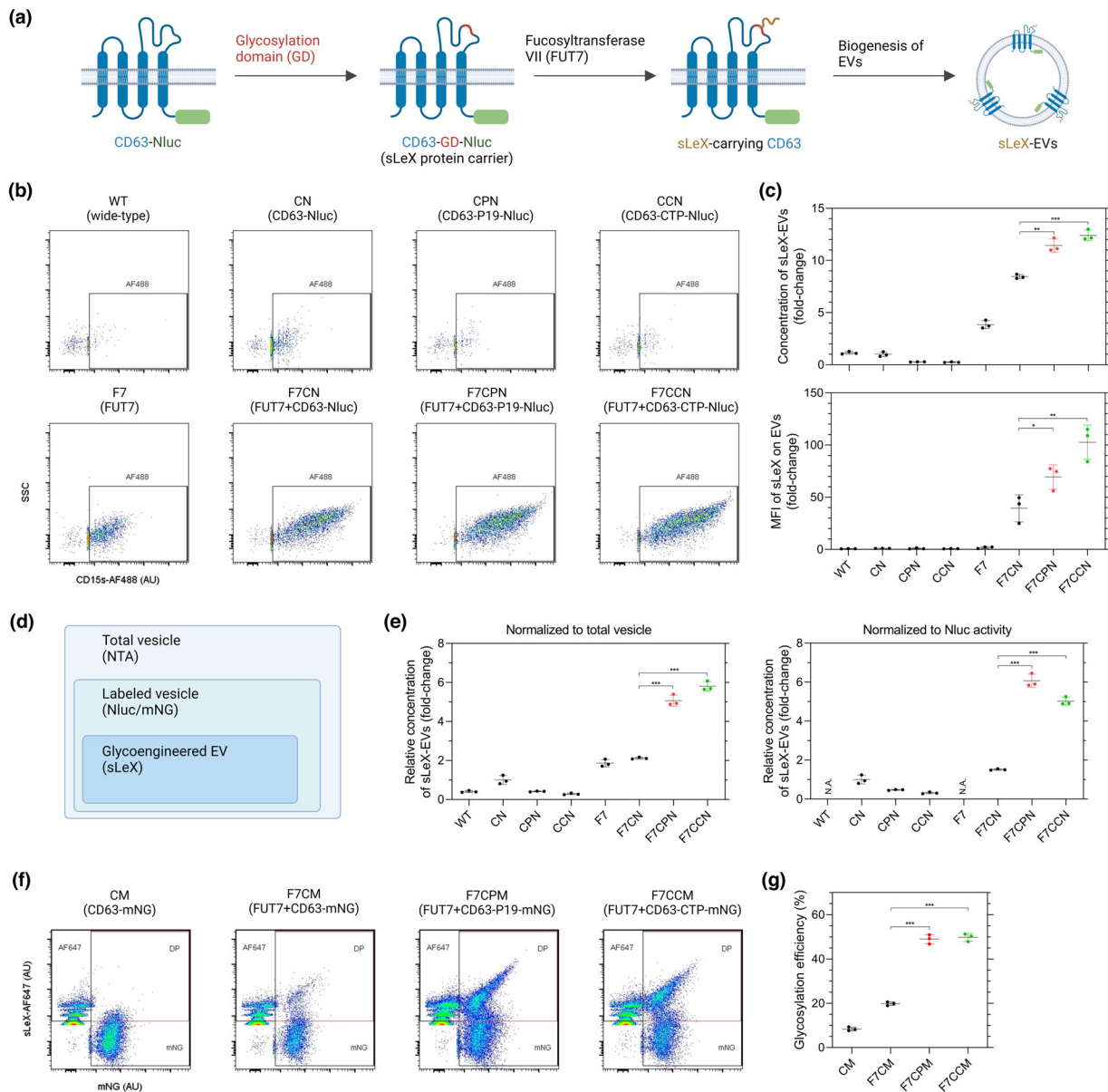


FIGURE 1 Engineering approach for surface display of sLeX on EVs. (a) Three-module design for glycoengineering. A glycosylation domain (GD, either P19 or CTP) was inserted into the large extracellular loop of CD63 to form a novel sLeX protein carrier. Fucosyltransferase VII (FUT7) subsequently catalyzed the synthesis of sLeX glycan. The luciferase Nluc was fused to the C-terminal of CD63 for labelling engineered EVs. (b) Detection of sLeX on EVs using single-vesicle imaging flow cytometry. (c) Relative quantification of sLeX expression on EVs in (b). The concentration of sLeX-EVs and mean fluorescence intensity (MFI) of sLeX per vesicle are shown in the upper and lower panel, respectively. Results were presented as fold-change over the group CN. $N = 3$. (d) Venn diagram showing the relationship between different EV subpopulations. (e) Relative concentration of sLeX-EVs against total vesicles (left) and Nluc-labeled EVs (right). $N = 3$. Results were presented as fold-change over the group CN. (f) Detection of sLeX on mNG-labelled EVs using single-vesicle imaging flow cytometry. (g) Percentage of sLeX-EVs on mNG-labelled EVs in (f). $N = 3$. Data are shown as mean \pm standard deviation. WT: wide-type; CN: CD63-Nluc; CPN: CD63-P19-Nluc; CCN: CD63-CTP-Nluc; F7: FUT7; F7CN: FUT7 + CD63-Nluc; F7CPN: FUT7 + CD63-P19-Nluc; F7CCN: FUT7 + CD63-CTP-Nluc; CM: CD63-mNG; F7CM: FUT7 + CD63-mNG; F7CPM: FUT7 + CD63-P19-mNG; F7CCM: FUT7 + CD63-CTP-mNG. Two-tailed unpaired *t*-test. * $p < 0.05$; ** $p < 0.01$; *** $p < 0.001$

Compared to adherent cells like HEK-293T, suspension cells represent a more convenient and up-scalable system for EV production due to simpler propagation procedures. To test the feasibility of the glycoengineering strategy in suspension cells, Freestyle 293-F cells were transduced and the EVs thereof were characterized. The results show that F7CPN and F7CCN EVs from suspension cells were alike to that from adherent cells in terms of size (Figure S4c), positivity for sLeX (Figure S4d), elution profile in SEC (Figure S4e), and binding to E-selectin (Figure S4f). Taken together, these results verify that surface display of sLeX on EVs conferred strong binding to E-selectin but did not affect the physicochemical characteristics.

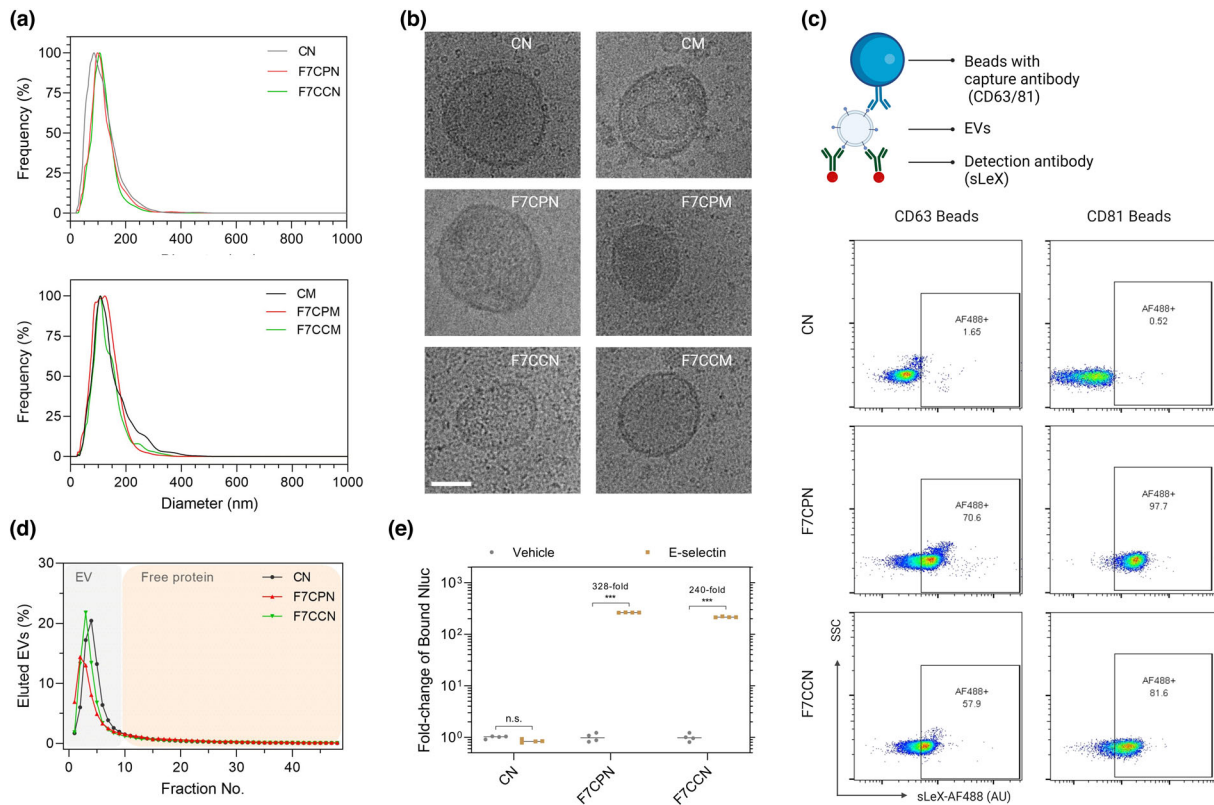


FIGURE 2 Physicochemical and functional characterization of sLeX-EVs. (a) Size distribution of Nluc and mNG-labelled EVs. (b) Cryo-electron microscopy images of Nluc and mNG-labelled EVs. Scale bar indicates 100 nm. (c) Detection of sLeX on Nluc-labelled EVs captured by CD63 and CD81-coated beads. EVs were pulled down using magnetic beads pre-coated with capture antibodies against an EV marker and detected with sLeX antibodies using flow cytometry. (d) Elution profile of Nluc-labelled EVs in size exclusion chromatography. Nluc in each fraction was normalized to total input. (e) Binding of Nluc-labelled EVs to recombinant E-selectin. Microplates were coated with E-selectin and incubated with EVs. The amount of bound EVs was presented as fold-change over vehicle-coated plates. Data are shown as mean \pm standard deviation. CN: CD63-Nluc; F7CPN: FUT7 + CD63-P19-Nluc; F7CCN: FUT7 + CD63-CTP-Nluc; CM: CD63-mNG; F7CPM: FUT7 + CD63-P19-mNG; F7CCM: FUT7 + CD63-CTP-mNG. Two-tailed unpaired *t*-test. n.s.: non-significant; ****p* < 0.001

3.3 | sLeX-EVs exhibit high specificity towards activated endothelial cells in vitro

Following ligand binding, E-selectin undergoes rapid internalization and mediates the endocytosis of sLeX-expressing nanoparticles (Jubeli et al., 2012; Setiadi & McEver, 2008). To examine the cellular uptake of sLeX-EVs, HUVEC (human umbilical vein endothelial cells) and HAEC (human artery endothelial cells) were first stimulated with TNF- α to induce E-selectin expression prior to treatment with EVs (Figures 3a and S5a). In both cell lines, we found similar levels of uptake of non-targeting Nluc-labelled EVs (i.e., CN) by un-activated and activated endothelial cells, whereas activated cells had significantly higher uptake of F7CPN (≥ 3.3 -fold) and F7CCN (≥ 4.2 -fold) compared to un-activated cells (Figure 3b). Similar to Nluc-based assay, treatment with mNG-labelled sLeX-EVs (i.e., F7CPM and F7CCM) induced a significant shift in the fluorescence intensity of activated cells compared to non-activated cells (Figure 3c), with the increases of cellular mNG intensity higher than 2.6-fold for HUVEC and 2.0-fold for HAEC, respectively (Figure 3d). Moreover, the enhancement was abrogated by blocking sLeX ligands (Figure S5b) and E-selectin receptors (Figure 3b) with corresponding antibodies, indicating the cellular uptake was mainly mediated by the sLeX-E-selectin axis.

Interestingly, endothelial uptake of sLeX-EVs became evident with incubation duration as short as 30 min (Figure 3e) and with a low EV dose ($4e^8$ /ml, Figure 3f). Besides flow cytometry, HUVEC cells were imaged using confocal microscopy to assess intracellular trafficking routes of internalized EVs. All types of EVs led to punctate mNG signals proximal to the lysosome in activated HUVEC cells (Figure 3g), suggesting a common endosome-lysosome internalization pathway. TNF- α activation also slightly enhanced the uptake of non-targeting mNG-labelled EVs (Figure 3d), which contrasts with Nluc-based assay. The discrepancy is likely attributable to a higher fraction of cell surface-associated EVs in un-activated cells versus activated counterparts, since cell surface-associated EVs were measured together with intracellular EVs in the Nluc-based assay but omitted in the mNG-based assay where trypsinization was used to prepare singlet cells.

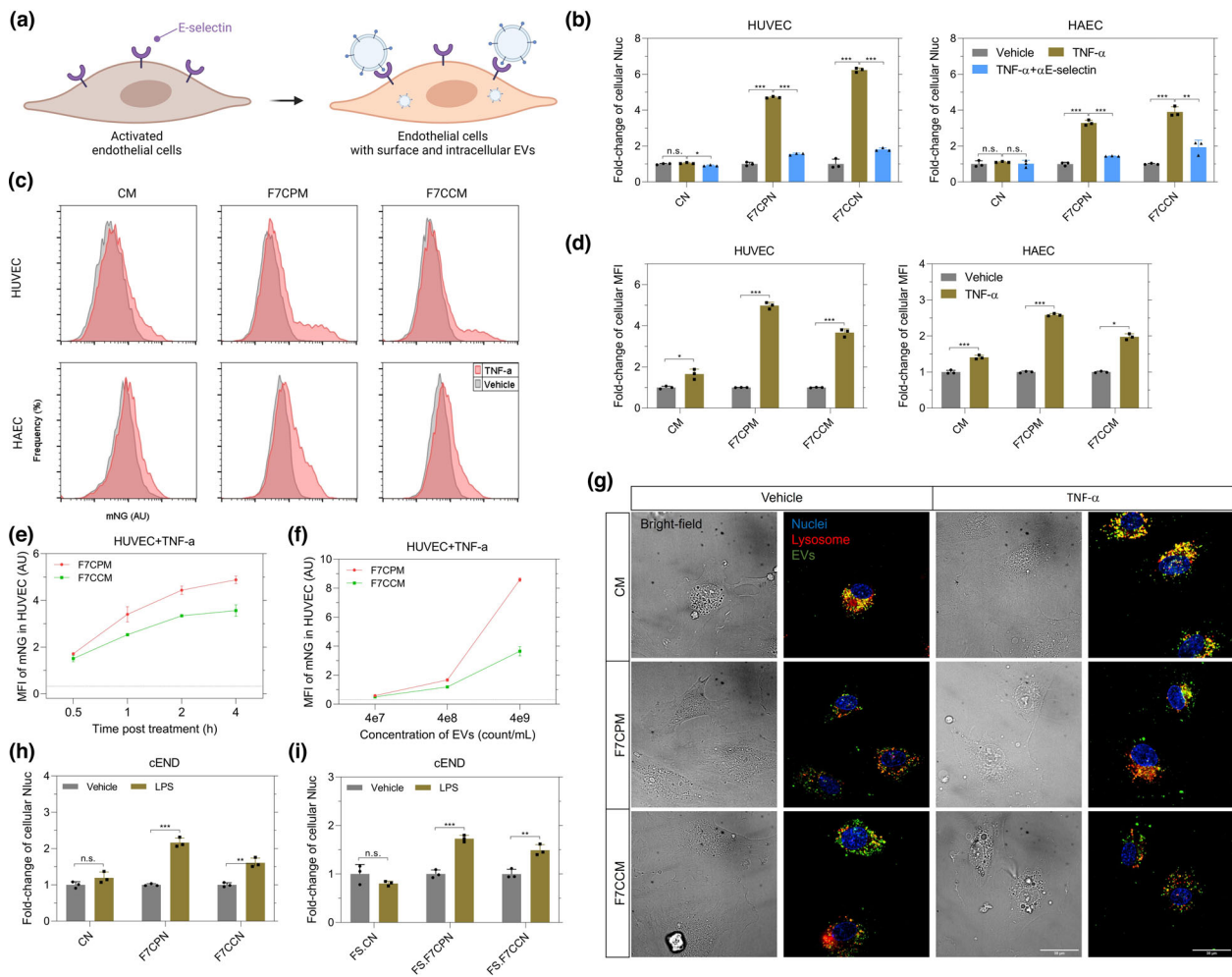


FIGURE 3 Uptake of sLeX-EVs by endothelial cells. (a) Scheme of analysis of cellular uptake. Endothelial cells were stimulated with TNF- α to induce E-selectin expression and treated with Nluc- and mNG-labelled EVs. In some settings, antibodies against sLeX and E-selectin were added along with EVs to block the ligand and receptor, respectively. (b) Relative quantification of cellular Nluc after treatment with 2e (Kwon et al., 2021)/mL EVs for 4 h. *N* = 3. (c-d) Histogram (c) and mean fluorescence intensity (MFI, d) of endothelial cells after treatment with 2e (Kwon et al., 2021)/ml EVs for 4 h. *N* = 3. (e) Effect of EV treatment duration on cellular mNG intensity. EV dose was 4e (Kwon et al., 2021)/mL. *N* = 3. (f) Effect of EV dose on cellular mNG intensity. Treatment duration was 4 h. *N* = 3. The dash lines in (e-f) indicate untreated cells. (g) Images of HUVEC cells after treatment with 2e (Kwon et al., 2021)/ml EVs for around 2 h. (h-i) Relative quantification of cellular Nluc in cEND cells after treatment with EVs from HEK-293T (h) or Freestyle 293-F (i) cells. cEND cells were stimulated with lipid polysaccharides (LPS) to induce E-selectin expression and treated with 2e (Kwon et al., 2021)/ml EVs for 4 h. *N* = 3. The amount of cellular EVs was presented as fold-change over vehicle-stimulated cells. Data are shown as mean \pm standard deviation. CN: CD63-Nluc; F7CPN: FUT7 + CD63-P19-Nluc; F7CCN: FUT7 + CD63-CTP-Nluc; CM: CD63-mNG; F7CPM: FUT7 + CD63-P19-mNG; F7CCM: FUT7 + CD63-CTP-mNG. FS.: Freestyle 293-F. Two-tailed unpaired *t*-test. n.s.: non-significant; **p* < 0.05; ***p* < 0.01; ****p* < 0.001

Human and mouse E-selectin are highly conserved, and both bind sLeX. Therefore, we assessed the uptake of sLeX-EVs in the mouse cerebral endothelial cell line cEND following activation with another common stimulating agent, lipid polysaccharide (LPS). As seen in human endothelial cells, activation of cEND cells improved the uptake of F7CPN and F7CCN but not non-targeting EVs (Figure 3h). In agreement with the enhanced binding to recombinant E-selectin, sLeX-EVs from FreeStyle 293-F cells had significantly higher Nluc in activated endothelial cells (Figures 3i and S5c). In general, surface display of sLeX on EVs improves their specificity towards activated endothelial cells.

3.4 | sLeX-EVs targeted endothelial cells in a murine model of colitis

The specificity of sLeX towards activated endothelial cells warrants evaluating whether the specific targeting could also be observed *in vivo*. E-selectin expression is commonly upregulated in inflammatory bowel disease in humans and can be modelled by picrylsulfonic acid-induced colitis in mice (Kawachi et al., 2000; Nong et al., 2022). Here, Nluc-labelled EVs were intravenously injected into colitis mice and their levels in tissues and plasma were quantified as previously reported by us (Figure 4a)

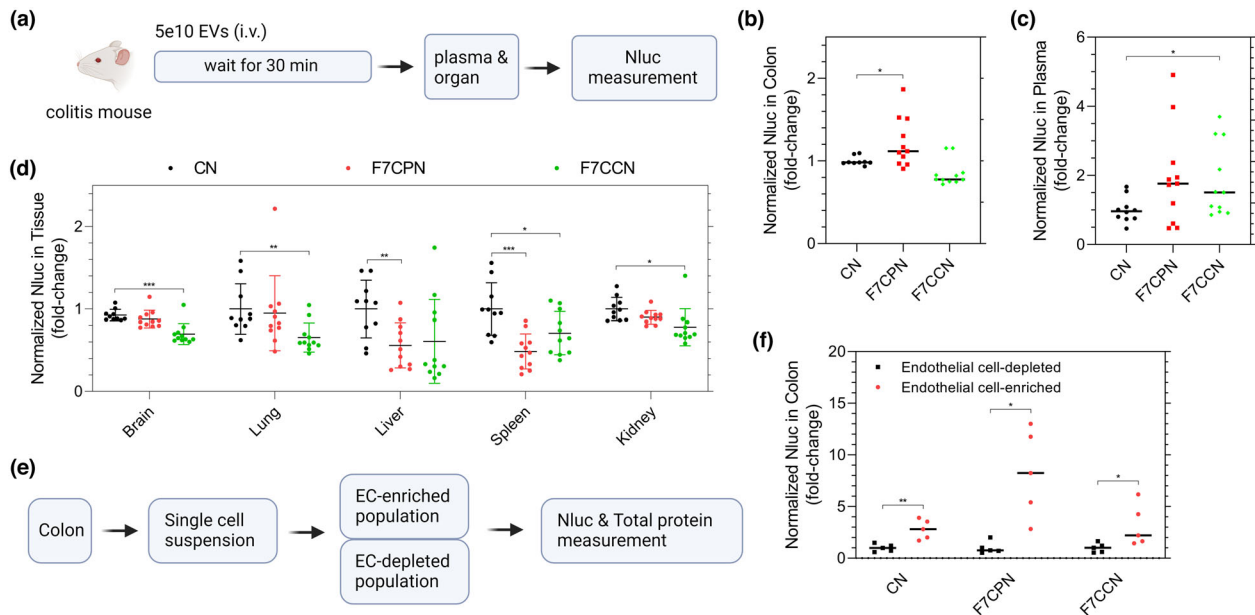


FIGURE 4 Uptake of sLeX-EVs in colitis mice. (a) Scheme of analysis of uptake in colitis mice. Colitis mice were established via instillation of picrylsulfonic acid in the rectum and injected with 5e (Y. Liang et al., 2021) Nluc-labelled EVs via tail veins. Tissues and plasma were dissected 30 min after injection and analyzed for Nluc levels. (b) Relative quantification of Nluc in the colon. (c) Relative quantification of Nluc in plasma. (d) Relative quantification of Nluc in major organs. In figure (b-d), the amount of EVs in tissues (per gram of wet tissue) and plasma (per μL of plasma) were normalized to total input and presented as fold-change over non-targeting EVs. $N = 9-11$. (e) Scheme of enriching endothelial cells from colon. (f) Relative quantification of Nluc in endothelial cell-enriched and -depleted fractions of colon cells. The amount of EVs in the fractions was normalized to total protein and presented as a fold-change over endothelial cell-depleted fraction. $N = 5$. Data are shown as mean \pm standard deviation. CN: CD63-Nluc; F7CPN: FUT7 + CD63-P19-Nluc; F7CCN: FUT7+ CD63-CTP-Nluc. Two-tailed unpaired *t*-test. n.s.: non-significant; * $p < 0.05$; ** $p < 0.01$; *** $p < 0.001$

(Gupta et al., 2020). Considering that intravenously administered EVs have been reported to be quickly cleared from plasma and activated endothelial cells had significant uptake of sLeX-EVs within a short time frame (Figure 3e), we selected 30 min as the endpoint for the in vivo study. Noteworthy, we found that F7CPN, but not F7CCN, had slightly (around 23%) but significantly higher accumulation in the colon compared to non-targeting EVs (Figure 4b). Sialylation is reported to extend the half-life of recombinant proteins and synthetic nanoparticles, which is likely attributable to terminal sialyl groups that reduce excretion in the kidney (Rosa et al., 1984). In our experiment, surface display of sLeX also increased the retention of EVs in plasma, with that of F7CCN being 1.8-fold higher than non-targeting EVs (Figure 4c). In addition, sLeX-EVs had significantly lower accumulation in several tissues including the scavenging tissues spleen and liver, which favours extrahepatic/splenic drug delivery (Figure 4d).

Next, we investigated whether EVs were enriched in activated endothelium. Since endothelial cells constitute a low percentage of tissue mass (around 2%), the endothelium-targeting effect might be outweighed by other cell populations and extracellular matrix. Therefore, we enriched endothelial cells using magnetic beads coated with antibodies against CD31, an endothelial marker (Figures S6a and 4e). Endothelial cell-depleted fractions were also collected to account for non-specific accumulation (Figure S6b). The results show that F7CPN and F7CCN had around 8.2- and 3.2-fold higher accumulation in the endothelial cell-enriched fraction than fractions without endothelial cells, while the fold-change of non-targeting EVs was less prominent (Figure 4f).

Many types of tumours are reported to have activated endothelial cells, thus we established subcutaneous B16F10 melanoma model in mice and quantified Nluc-labelled sLeX-EVs in the tumour, plasma, and major tissues following intravenous injection of EVs. However, we did not detect greater accumulation of sLeX-EVs in the tumour compared to non-targeting EVs (Figure S6c), which is probably due to the absence of E-selectin expression. Similar to the result in the colitis model, significant decreases in hepatic and splenic accumulation and extension of plasma retention were observed. Taken together, these data implicate that surface display of sLeX on EVs improves targeting to colon endothelial cells in colitis mice.

3.5 | sLeX-EVs from MSCs attenuate endothelial damage

Building on the endothelial-targeting ability of sLeX-EVs, we sought to endow EVs with therapeutic activity. Therefore, the same glycoengineering approach was applied to cord blood-derived MSCs that are reported to have anti-inflammatory properties (Börger et al., 2020; Liao et al., 2016). Three stable cell lines were established from MSCs using lentiviral transduction and the EVs thereof were assessed for their ability to target endothelial cells and attenuate endothelial damage.

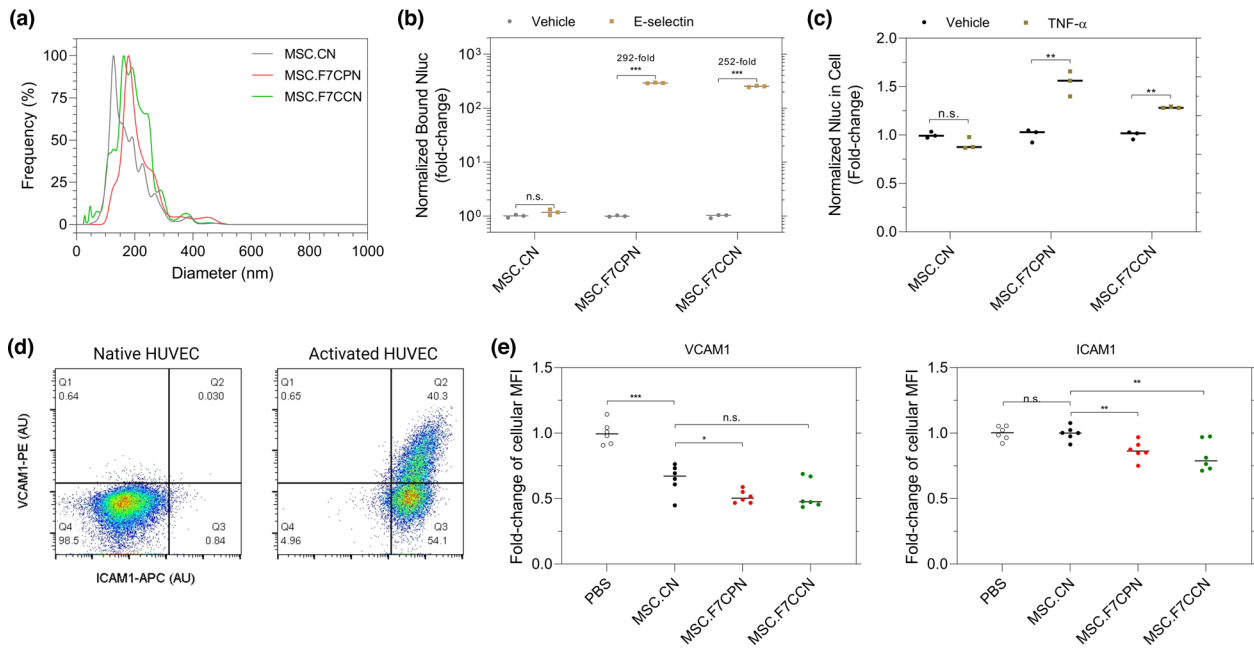


FIGURE 5 Endothelial repair with EVs from mesenchymal stem cells. (a) Size distribution of mesenchymal stem cells-derived EVs. (b) Binding of Nluc-labelled EVs to recombinant E-selectin. Microplates were coated with E-selectin and incubated with EVs for 2 h. The amount of bound EVs were presented as fold-change over vehicle-coated plates. $N = 3$. (c) Relative quantification of cellular Nluc after treatment with $2e$ (Kwon et al., 2021)/ml EVs for 4 h. The amount of cellular EVs was presented as fold-change over vehicle-stimulated HUVEC cells. $N = 3$. (d) Expression of endothelial damage markers on TNF- α -activated HUVEC cells. (e) Relative quantification of VCAM1 and ICAM1 expression on HUVEC cells. The level of cellular MFI was presented as fold-change over PBS-treated cells. $N = 6$. Data are shown as mean \pm standard deviation. MSC.CN: CD63-Nluc from MSCs; MSC.F7CPN: FUT7 + CD63-P19-Nluc from MSCs; MSC.F7CCN: FUT7+ CD63-CTP-Nluc from MSCs. Two-tailed unpaired t -test. n.s.: non-significant; * $p < 0.05$; ** $p < 0.01$; *** $p < 0.001$

Characterization using NTA shows that the EVs from MSCs had mode diameters around 120 nm with narrow size distribution (Figure 5a). Like the EVs from HEK-293T cells, surface display of sLeX on MSCs-derived EVs resulted in significant binding to recombinant E-selectin (Figure 5b) as well as enhanced uptake by activated HUVEC cells (Figure 5c).

In addition to E-selectin, TNF- α stimulated the expression of two adhesion molecules VCAM1 and ICAM1 (Figure 5d) which are common surface markers of endothelial damage. Hence, they were used as the surrogate marker amid characterization of the endothelial repair efficacy of MSC-derived EVs. Notably, F7CPN and F7CCN demonstrated higher efficacy than non-targeting EVs in downregulating the expression of VCAM1 and ICAM1 (Figure 5e), suggestive of potential activity in amelioration of inflammation. Overall, combining the active targeting ability of sLeX-EVs and the intrinsic anti-inflammatory activity of MSCs achieves higher efficacy to attenuate endothelial damage.

3.6 | The use of a different fucosyltransferase produces EVs with dendritic cell-targeting ability

Unlike FUT7, fucosyltransferase IX (FUT9) prefers to catalyze fucosylation of the N-acetylglucosamine (GlcNAc) of a distal alpha 2,3 asialylated lactosamine unit, thus forming Lewis X (LeX) antigen (Lowe, 2002; Schneider et al., 2017). Previous studies found that the combination of FUT9 and PSGL-1 resulted in the highest expression of Lewis X (LeX) but not sLeX (Lo et al., 2013; Mondal et al., 2018). Moreover, dendritic cells constitutively express DC-SIGN (DC-specific intercellular adhesion molecule-3 grabbing non-integrin) on the surface and internalize LeX-expressing pathogens and vesicles (Dusoswa et al., 2019; Schettters et al., 2018). As such, we assumed that FUT9 might be combined with CD63-GD-Nluc for surface display of LeX, producing EVs capable of targeting dendritic cells.

HEK-293T cells were transfected using the same strategy as above for producing LeX-EVs (Figure 6a). In accordance with our design, the combination of FUT9 and either GD (P19 or CTP) produced EVs with surface LeX (Figure 6b). The size of LeX-EVs were narrowly distributed with a mode diameter around 110 nm (Figure 6c). As described above, we first precluded the presence of free Nluc proteins in the EV preparations via examining their elution profiles on size exclusion chromatography, and the single peak in the typical EV elution fractions corresponded to engineered EVs (Figure 6d). Using Nluc activity as the surrogate measurement, we found that surface display of LeX on EVs conferred around 20-fold increases in the binding to recombinant human DC-SIGN (Figure 6e).

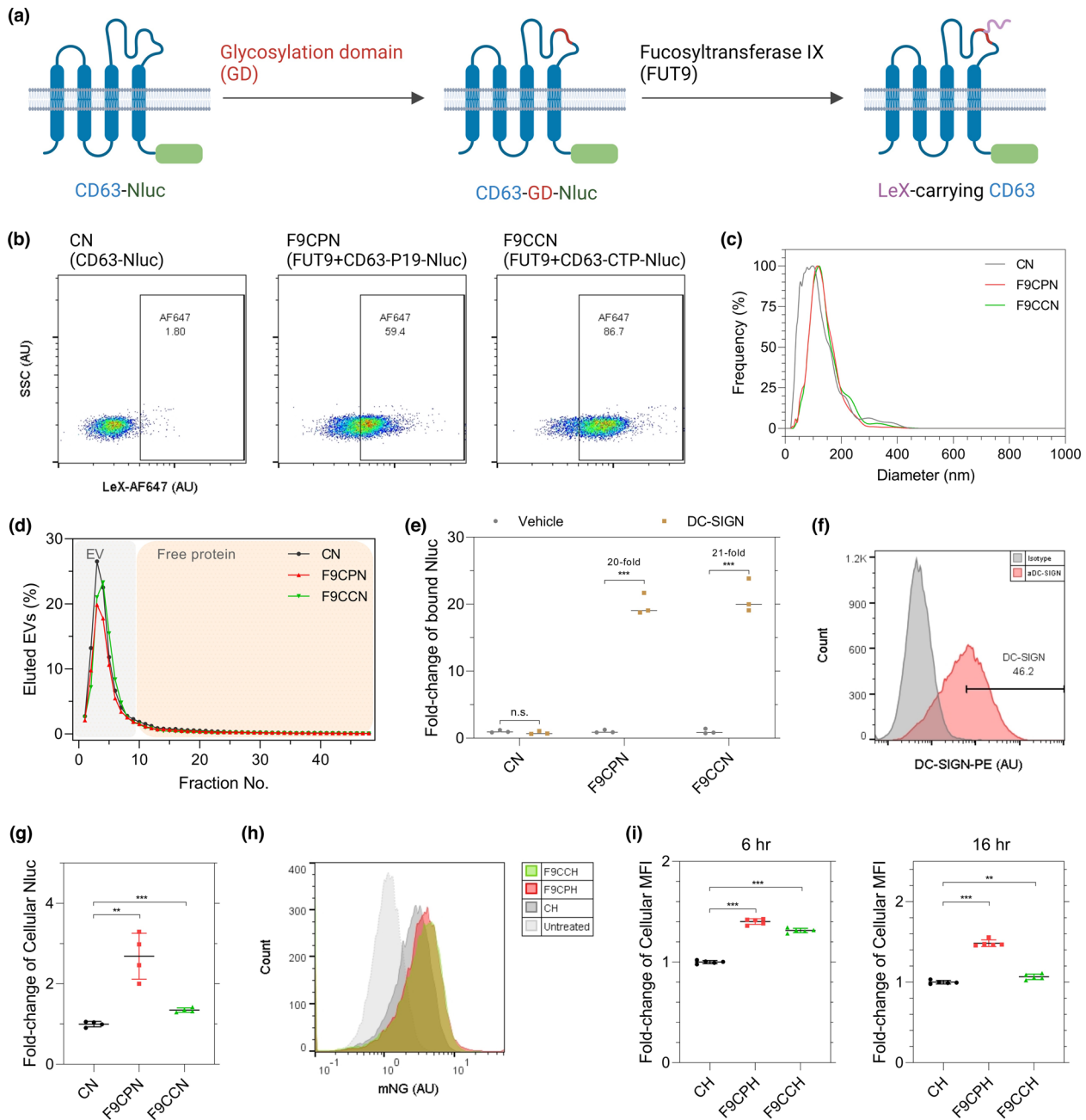


FIGURE 6 Production and cellular uptake of LeX-EVs. (a) Scheme of surface display of LeX on CD63. A glycosylation domain (GD) was inserted to the large extracellular loop of CD63 to form a novel sLeX protein carrier. Fucosyltransferase IX (FUT9) subsequently catalyzed the synthesis of LeX glycan. The luciferase Nluc was fused to the C-terminal of CD63 for labelling engineered EVs. (b) Detection of LeX on EVs captured by CD63-coated beads. (c) Size distribution profile of EVs. (d) Elution profile of Nluc-labelled EVs in size exclusion chromatography. Nluc in each fraction was normalized to total input. (e) Binding of Nluc-labelled EVs to recombinant human DC-SIGN. Microplates were coated with human DC-SIGN and incubated with EVs for 2 h. The amount of bound EVs were presented as fold-change over vehicle-coated plates. $N = 3$. (f) Expression of DC-SIGN on mouse bone marrow-derived dendritic cells (mBMDCs). (g) Relative quantification of cellular Nluc in mBMDCs after treatment with 2e⁸ (Kwon et al., 2021)/ml EVs for 6 h. $N = 4$. (h) Histogram of mBMDCs after treatment with the same amount of HiBiT-mNG-labeled EVs for 6 h. (i) Relative quantification of cellular MFI after treatment with the same amount of HiBiT-mNG-labeled EVs for 6 h or 16 h. $N = 5$. The amount of cellular EVs in (g) and (i) were presented as fold-change over non-targeting EVs. Data are shown as mean \pm standard deviation. CN: CD63-Nluc; F9CPN: FUT9 + CD63-P19-Nluc; F9CCN: FUT9 + CD63-CTP-Nluc. CH: CD63-mNG-HiBiT; F9CPH: FUT9 + CD63-P19-mNG-HiBiT; F9CCH: FUT9 + CD63-CTP-mNG-HiBiT. Two-tailed unpaired *t*-test. n.s.: non-significant; ** $p < 0.01$; *** $p < 0.001$

To examine the cellular uptake of LeX-EVs, we established mouse bone marrow-derived dendritic cells (mBMDCs, Figure S7a) and confirmed expression of DC-SIGN on the cell surface (Figure 6f). Aligning with our assumption, LeX-EVs were more efficiently internalized by mBMDCs compared to non-targeting EVs (Figure 6g). To detect the amount of internalized EVs at a single-cell level, Nluc was replaced with a hybrid reporter HiBiT-mNG (Figure S7b) in which the 8-mer peptide HiBiT regains luciferase activity upon complementation with the remaining subunit provided in the assay kit. mBMDCs were treated with the

same amount of labelled EVs (on the basis of HiBiT measurement) and analyzed by flow cytometry (Figure 6h). Similar to the Nluc-based assay, LeX-EVs induced significantly higher fluorescence intensity in mBMDCs than non-targeting EVs (Figures 6i and S7c), suggesting improved cellular uptake. Overall, these results substantiate the ability of LeX-EVs to target dendritic cells and the adaptability of our modular engineering design.

4 | DISCUSSION

To date, a variety of proteins and peptides have been displayed on EV surface to improve the cellular specificity. In this study, we expand the toolset by pioneering use of glycan ligands for targeting EVs to activated endothelial cells and dendritic cells. Surface display of glycan ligands was achieved through a novel glycoengineering strategy consisting of three reconfigurable modules: (a) an EV scaffold protein amenable for surface display, (b) a GD as the glycan carrier, and (c) a glycosyltransferase for synthesis of the glycan of interest.

CD63 is a well-characterized EV scaffold protein and was used as the model system for surface display. Besides CD63, our group and others have shown that the small and large extracellular loops of other tetraspanin proteins (such as CD9 and CD81) and the extracellular domain of single-pass transmembrane proteins (such as Lamp2b and PTGFRN) are also amenable for surface display of functional moieties (Corso et al., 2019; Dooley et al., 2021). Not only full-length proteins, but also truncated proteins and transmembrane domains are potential candidate modules of the glycoengineering strategy (Curley et al., 2020), but knowledge about the relative efficiency of those proteins/domains is limited. Building on the results here, it would be interesting to investigate other scaffold proteins and domains for the display of glycan ligands.

Although the large extracellular domain of CD63 has been reported to be permissive for full-length mNG (253aa) (Corso et al., 2019), in our design two peptides of 19–28 amino acids were selected as the GDs, which was assumed to facilitate protein expression. The high efficiency of both peptides as glycan carriers underline the robustness of our glycoengineering strategy. Interestingly, the two domains appear to confer slightly different biological properties in terms of cellular targeting and plasma retention. For instance, P19 tended to have higher cellular targeting effect for both sLeX-EVs and LeX-EVs, but CTP was more efficient to extend retention of EVs in plasma. Mechanisms underlying the discrepancy remain unknown but might include different levels of O-glycosylation and structural uniqueness. To further boost cellular uptake, we sought to improve sLeX density on the EV surface by means of having more repeats of the P19 peptide in CD63. Albeit still outperforming non-targeting EVs, the fold increase of cellular Nluc for sLeX-EVs carrying two or four repeats of P19 (F7CP₂N and F7CP₄N) was less than for one repeat (Figure S5d). In future, more potent GDs might be identified through genetic screening and machine learning.

With the same GD, switching the glycosyltransferase from FUT7 to FUT9 readily produces EVs with distinct glycan ligands (from sLeX and LeX) and target cell types (from endothelial cells to dendritic cells), highlighting the flexibility of the glycoengineering design. The vast variety of glycosyltransferases available could potentially be harnessed for surface display of glycans with distinct biological functions (Gerlach & Griffin, 2016; Hung & Leonard, 2015; Martins et al., 2021; Shinnakasu et al., 2021; Spence et al., 2015).

The endothelium-targeting ability of sLeX-EVs was successfully combined with the inherent therapeutic activity of MSCs-derived EVs in the context of endothelial damage in cell culture models. Knowledge acquired from studies to improve the yield of EVs like gel coating, cytokine stimulation and alternative MSC sources could be applied in future, so that the therapeutic efficacy thereof could be tested in vivo. Similar to sLeX-EVs, the suitability of LeX-EVs for the delivery of antigens like tumour neoantigens, viral components, or self-antigens to dendritic cells warrants further exploration.

In conclusion, this study presents a novel glycoengineering strategy for surface display of sLeX and LeX on EVs and validates the specificity of the glycoengineered EVs to activated endothelial cells and dendritic cells, respectively. Furthermore, the modularity of our glycoengineering design holds promises for further adaptation in terms of cellular specificity and loading therapeutic molecules.

AUTHOR CONTRIBUTIONS

Wenyi Zheng: Conceptualization; Data curation; Investigation; Methodology; Project administration; Writing – original draft. Rui He: Data curation; Resources. Xiuming Liang: Investigation. Samantha Roudi: Data curation; Investigation. Jeremy Bost: Investigation. Pierre-Michael Coly: Data curation. Guillaume van Niel: Investigation. Samir E. L. Andaloussi: Funding acquisition; Investigation; Project administration; Resources; Supervision; Writing – review & editing

ACKNOWLEDGEMENTS

We thank Dave Carter, Tony De Fougères, and David Lowe for editing the manuscript. S.E.-A. is supported by H2020 EXPERT (No. 825828), the Swedish foundation of Strategic Research (SSF-IRC; FormulaEx IRC15-0065), ERC CoG DELIVER (No. 101001374), the Swedish Medical Research Council (VR-Med 2020-01322), and EVOX Therapeutics Ltd. PMC is funded by Institut National Du Cancer grant (INCA N° 2019-125 PLBIO19-059) and GvN by ANR ZENITH (ANR-20-CE18-0026_01).

CONFLICT OF INTEREST

SEA is founding consultant for and have equity interests in EVOX Therapeutics Ltd., Oxford, UK. The other authors declare no competing financial interests.

DATA AVAILABILITY STATEMENT

The authors declare that the data supporting the findings of this study are available within the paper and its supplementary information files.

ORCID

Wenyi Zheng  <https://orcid.org/0000-0003-2416-5822>

Xiuming Liang  <https://orcid.org/0000-0003-0202-1211>

Guillaume van Niel  <https://orcid.org/0000-0002-8651-9705>

REFERENCES

- Alvarez-Erviti, L., Seow, Y., Yin, H., Betts, C., Lakhali, S., & Wood, M. J. (2011). Delivery of siRNA to the mouse brain by systemic injection of targeted exosomes. *Nature Biotechnology*, 29, 341–345. <https://doi.org/10.1038/nbt.1807>
- Börger, V., Weiss, D. J., Anderson, J. D., Borràs, F. E., Bussolati, B., Carter, D. R. F., Dominici, M., Falcón-Pérez, J. M., Gimona, M., Hill, A. F., Hoffman, A. M., de Kleijn, D., Levine, B. L., Lim, R., Lötval, J., Mitsialis, S. A., Monguió-Tortajada, M., Muraca, M., Nieuwland, R., ..., Giebel, B. (2020). ISEV and ISCT statement on EVs from MSCs and other cells: Considerations for potential therapeutic agents to suppress COVID-19. *Cytotherapy*, 22, 482–485. <https://doi.org/10.1016/j.jcyt.2020.05.002>
- Buffone, A., Mondal, N., Gupta, R., McHugh, K. P., Lau, J. T., & Neelamegham, S. (2013). Silencing α 1,3-fucosyltransferases in human leukocytes reveals a role for FUT9 enzyme during e-selectin-mediated cell adhesion. *Journal of Biological Chemistry*, 288, 1620–1633. <https://doi.org/10.1074/jbc.M112.400929>
- Ceaglio, N., Gugliotta, A., Tardivo, M. B., Cravero, D., Etcheverrigaray, M., Kratje, R., & Oggero, M. (2016). Improvement of in vitro stability and pharmacokinetics of hIFN- α by fusing the carboxyl-terminal peptide of hCG β -subunit. *Journal of Biotechnology*, 221, 13–24. <https://doi.org/10.1016/j.jbiotec.2016.01.018>
- Corso, G., Heusermann, W., Trojer, D., Görgens, A., Steib, E., Voshol, J., Graff, A., Genoud, C., Lee, Y., Hean, J., Nordin, J. Z., Wiklander, O. P. B., El Andaloussi, S., & Meisner-Kober, N. (2019). Systematic characterization of extracellular vesicles sorting domains and quantification at the single molecule–single vesicle level by fluorescence correlation spectroscopy and single particle imaging. *Journal of Extracellular Vesicles*, 8, 1663043. <https://doi.org/10.1080/20013078.2019.1663043>
- Curley, N., Levy, D., Do, M. A., Brown, A., Stickney, Z., Marriott, G., & Lu, B. (2020). Sequential deletion of CD63 identifies topologically distinct scaffolds for surface engineering of exosomes in living human cells. *Nanoscale*, 1. <https://doi.org/10.1039/D0NR00362J>
- Dooley, K., McConnell, R. E., Xu, K., Lewis, N. D., Haupt, S., Younis, M. R., Martin, S., Sia, C. L., McCoy, C., Moniz, R. J., Burenkova, O., Sanchez-Salazar, J., Jang, S. C., Choi, B., Harrison, R. A., Houde, D., Burzyn, D., Leng, C., Kirwin, K., ..., Williams, D. E. (2021). A versatile platform for generating engineered extracellular vesicles with defined therapeutic properties. *Molecular Therapy*, 29, 1729–1743. <https://doi.org/10.1016/j.ymthe.2021.01.020>
- Dusowska, S. A., Horrevorts, S. K., Ambrosini, M., Kalay, H., Paaau, N. J., Nieuwland, R., Pegtel, M. D., Würdinger, T., Van Kooyk, Y., & Garcia-Vallejo, J. J. (2019). Glycan modification of glioblastoma-derived extracellular vesicles enhances receptor-mediated targeting of dendritic cells. *Journal of Extracellular Vesicles*, 8, 1648995. <https://doi.org/10.1080/20013078.2019.1648995>
- Fu, W., Lei, C., Liu, S., Cui, Y., Wang, C., Qian, K., Li, T., Shen, Y., Fan, X., Lin, F., Ding, M., Pan, M., Ye, X., Yang, Y., & Hu, S. (2019). CAR exosomes derived from effector CAR-T cells have potent antitumour effects and low toxicity. *Nature Communications*, 10. <https://doi.org/10.1038/s41467-019-12321-3>
- Gao, X., Ran, N., Dong, X., Zuo, B., Yang, R., Zhou, Q., Moulton, H. M., Seow, Y., & Yin, H. (2018). Anchor peptide captures, targets, and loads exosomes of diverse origins for diagnostics and therapy. *Science Translational Medicine*, 10. <https://doi.org/10.1126/scitranslmed.aat0195>
- Gerlach, J. Q., & Griffin, M. D. (2016). Getting to know the extracellular vesicle glycome. *Molecular Biosystems*, 12, 1071–1081. <https://doi.org/10.1039/C5MB00835B>
- Görgens, A., Corso, G., Hagey, D. W., Jawad Wiklander, R., Gustafsson, M. O., Felldin, U., Lee, Y., Bostancioglu, R. B., Sork, H., Liang, X., Zheng, W., Mohammad, D. K., van de Wakker, S. I., Vader, P., Zickler, A. M., Mamand, D. R., Ma, L., Holme, M. N., Stevens, M. M., ..., El Andaloussi, S. (2022). Identification of storage conditions stabilizing extracellular vesicles preparations. *Journal of Extracellular Vesicles*, 11, e12238. <https://doi.org/10.1002/jev2.12238>
- Gupta, D., Liang, X., Pavlova, S., Wiklander, O. P. B., Corso, G., Zhao, Y., Saher, O., Bost, J., Zickler, A. M., Piffko, A., Maire, C. L., Ricklefs, F. L., Gustafsson, O., Llorente, V. C., Gustafsson, M. O., Bostancioglu, R. B., Mamand, D. R., Hagey, D. W., Görgens, A., ..., El Andaloussi, S. (2020). Quantification of extracellular vesicles in vitro and in vivo using sensitive bioluminescence imaging. *Journal of Extracellular Vesicles*, 9, 1800222. <https://doi.org/10.1080/20013078.2020.1800222>
- Henseleit, U., Steinbrink, K., Goebeler, M., Roth, J., Vestweber, D., Sorg, C., & Sunderkötter, C. (1996). E-selectin expression in experimental models of inflammation in mice. *Journal of Pathology*, 180, 317–325. [10.1002/\(SICI\)1096-9896\(199611\)180:3<317::AID-PATH670>3.0.CO;2-O](https://doi.org/10.1002/(SICI)1096-9896(199611)180:3<317::AID-PATH670>3.0.CO;2-O)
- Hong, S., Yu, C., Wang, P., Shi, Y., Cao, W., Cheng, B., Chapla, D. G., Ma, Y., Li, J., Rodrigues, E., Narimatsu, Y., Yates, J. R., 3rd, Chen, X., Clausen, H., Moremen, K. W., Maccauley, M. S., Paulson, J. C., & Wu, P. (2020). Glycoengineering of NK cells with glycan ligands of CD22 and selectins for B-cell lymphoma therapy. *bioRxiv* 2020.03.23.004325.
- Hung, M. E., & Leonard, J. N. (2015). Stabilization of exosome-targeting peptides via engineered glycosylation. *Journal of Biological Chemistry*, 290, 8166–8172. <https://doi.org/10.1074/jbc.M114.621383>
- Jia, X., Tang, J., Yao, C., & Yang, D. (2021). Recent progress of extracellular vesicle engineering. *ACS Biomaterials Science & Engineering*, 7, 4430–4438. <https://doi.org/10.1021/acsbomaterials.1c00868>
- Johnson, L. R., Lee, D. Y., Eacret, J. S., Ye, D., June, C. H., & Minn, A. J. (2021). The immunostimulatory RNA RN7SL1 enables CAR-T cells to enhance autonomous and endogenous immune function. *Cell*, 184, 4981–4995. e14. <https://doi.org/10.1016/j.cell.2021.08.004>
- Jubeli, E., Moine, L., Vergnaud-Gauduchon, J., & Barratt, G. (2012). E-selectin as a target for drug delivery and molecular imaging. *Journal of Controlled Release*, 158, 194–206. <https://doi.org/10.1016/j.jconrel.2011.09.084>
- Kalluri, R., & LeBleu, V. S. (2020). The biology, function, and biomedical applications of exosomes. *Science* (80-), 367. <https://doi.org/10.1126/science.aau6977>
- Kawachi, S., Morise, Z., Conner, E., Laroux, F. S., Gray, L., Fuseler, J., & Grisham, M. B. (2000). E-selectin expression in a murine model of chronic colitis. *Biochemical and Biophysical Research Communications*, 268, 547–552. <https://doi.org/10.1006/bbrc.2000.2175>

- Kwon, S., Shin, S., Do, M., Oh, B. H., Song, Y., Bui, V. D., Lee, E. S., Jo, D. G., Cho, Y. W., Kim, D. H., & Park, J. H. (2021). Engineering approaches for effective therapeutic applications based on extracellular vesicles. *Journal of Controlled Release*, 330, 15–30. <https://doi.org/10.1016/j.jconrel.2020.11.062>
- Liang, X., Niu, Z., Galli, V., Howe, N., Zhao, Y., Wiklander, O. P. B., Zheng, W., Wiklander, R. J., Corso, G., Davies, C., Hean, J., Kyriakopoulou, E., Mamand, D. R., Amin, R., Nordin, J. Z., Gupta, D., & Andaloussi, S. E. (2022). Extracellular vesicles engineered to bind albumin demonstrate extended circulation time and lymph node accumulation in mouse models. *Journal of Extracellular Vesicles*, 11, e12248. <https://doi.org/10.1002/jev2.12248>
- Liang, Y., Duan, L., Lu, J., & Xia, J. (2021). Engineering exosomes for targeted drug delivery. *Theranostics*, 11, 3183–3195. <https://doi.org/10.7150/thno.52570>
- Liao, W., Pham, V., Liu, L., Riazifar, M., Pone, E. J., Zhang, S. X., Ma, F., Lu, M., Walsh, C. M., & Zhao, W. (2016). Mesenchymal stem cells engineered to express selectin ligands and IL-10 exert enhanced therapeutic efficacy in murine experimental autoimmune encephalomyelitis. *Biomaterials*, 77, 87–97. <https://doi.org/10.1016/j.biomaterials.2015.11.005>
- Lo, C. Y., Antonopoulos, A., Dell, A., Haslam, S. M., Lee, T., & Neelamegham, S. (2013). The use of surface immobilization of P-selectin glycoprotein ligand-1 on mesenchymal stem cells to facilitate selectin mediated cell tethering and rolling. *Biomaterials*, 34, 8213–8222. <https://doi.org/10.1016/j.biomaterials.2013.07.033>
- Lowe, J. B. (2002). Glycosylation in the control of selectin counter-receptor structure and function. *Immunological Reviews*, 186, 19–36. <https://doi.org/10.1034/j.1600-065X.2002.18603.x>
- Martins, Á. M., Ramos, C. C., Freitas, D., & Reis, C. A. (2021). Glycosylation of cancer extracellular vesicles: Capture strategies, functional roles and potential clinical applications. *Cells*, 10, 109. <https://doi.org/10.3390/cells10010109>
- Mondal, N., Dykstra, B., Lee, J., Ashline, D. J., Reinhold, V. N., Rossi, D. J., & Sackstein, R. (2018). Distinct human (1,3)-fucosyltransferases drive Lewis-X/sialyl Lewis-X assembly in human cells. *Journal of Biological Chemistry*, 293, 7300–7314. <https://doi.org/10.1074/jbc.RA117.000775>
- Nong, J., Glassman, P. M., & Muzykantov, V. R. (2022). Targeting vascular inflammation through emerging methods and drug carriers. *Advanced Drug Delivery Reviews*, 184, 114180. <https://doi.org/10.1016/j.addr.2022.114180>
- Panda, B., Sharma, Y., Gupta, S., & Mohanty, S. (2021). Mesenchymal stem cell-derived exosomes as an emerging paradigm for regenerative therapy and nanomedicine: A comprehensive review. *Life*, 11, 784. <https://doi.org/10.3390/life11080784>
- Richter, M., Vader, P., & Fuhrmann, G. (2021). Approaches to surface engineering of extracellular vesicles. *Advanced Drug Delivery Reviews*, 173, 416–426. <https://doi.org/10.1016/j.addr.2021.03.020>
- Rosa, C., Amr, S., Birken, S., Wehmann, R., & Nisula, B. (1984). Effect of desialylation of human chorionic gonadotropin on its metabolic clearance rate in humans. *Journal of Clinical Endocrinology and Metabolism*, 59, 1215–1219. <https://doi.org/10.1210/jcem-59-6-1215>
- Schetters, S. T. T., Kruijssen, L. J. W., Crommentuijn, M. H. W., Kalay, H., Ochando, J., den Haan, J. M. M., Garcia-Vallejo, J. J., & van Kooyk, Y. (2018). Mouse DC-SIGN/CD209a as target for antigen delivery and adaptive immunity. *Frontiers in Immunology*, 9, 10.3389/fimmu.2018.00990
- Setiadi, H., & McEver, R. P. (2008). Clustering endothelial E-selectin in clathrin-coated pits and lipid rafts enhances leukocyte adhesion under flow. *Blood*, 111, 1989–1998. <https://doi.org/10.1182/blood-2007-09-113423>
- Shinnakasu, R., Sakakibara, S., Yamamoto, H., Wang, P. H., Moriyama, S., Sax, N., Ono, C., Yamanaka, A., Adachi, Y., Onodera, T., Sato, T., Shinkai, M., Suzuki, R., Matsuura, Y., Hashii, N., Takahashi, Y., Inoue, T., Yamashita, K., & Kurosaki, T. (2021). Glycan engineering of the SARS-CoV-2 receptor-binding domain elicits cross-neutralizing antibodies for SARS-related viruses. *Journal of Experimental Medicine*, 218. <https://doi.org/10.1084/jem.20211003>
- Spence, S., Greene, M. K., Fay, F., Hams, E., Saunders, S. P., Hamid, U., Fitzgerald, M., Beck, J., Bains, B. K., Smyth, P., Themistou, E., Small, D. M., Schmid, D., O’Kane, C. M., Fitzgerald, D. C., Abdelghany, S. M., Johnston, J. A., Fallon, P. G., Burrows, J. F., ..., Scott, C. J. (2015). Targeting siglecs with a sialic acid-decorated nanoparticle abrogates inflammation. *Science Translational Medicine*. <https://doi.org/10.1126/scitranslmed.aab3459>
- Stahn, R., Goletz, S., Stahn, R., Wilmanowski, R., Wang, X., Briese, V., Friese, K., & Jeschke, U. (2005). Human chorionic gonadotropin (hCG) as inhibitor of E-selectin-mediated cell adhesion. *Anticancer Research*, 25, 1811–1816.
- Stahn, R., Schäfer, H., Kernchen, F., & Schreiber, J. (1998). Multivalent sialyl lewis x ligands of definite structures as inhibitors of E-selectin mediated cell adhesion. *Glycobiology*, 8, 311–319. <https://doi.org/10.1093/glycob/8.4.311>
- Teng, F., & Fussenegger, M. (2021). Shedding light on extracellular vesicle biogenesis and bioengineering. *Advancement of Science*, 8, 1–17. <https://doi.org/10.1002/advs.202003505>
- Wang, Z., Popowski, K. D., Zhu, D., de Juan Abad, B. L., Wang, X., Liu, M., Lutz, H., De Naeyer, N., DeMarco, C. T., Denny, T. N., Dinh, P. C., Li, Z., & Cheng, K. (2022). Exosomes decorated with a recombinant SARS-CoV-2 receptor-binding domain as an inhalable COVID-19 vaccine. *Nature Biomedical Engineering*, 6, 791–805. <https://doi.org/10.1038/s41551-022-00902-5>
- Wiklander, O. P. B., Brennan, M., Lötval, J., Breakefield, X. O., & Andaloussi, S. E. L. (2019). Advances in therapeutic applications of extracellular vesicles. *Science Translational Medicine*, 11, 1–16. <https://doi.org/10.1126/scitranslmed.aav8521>
- Williams, C., Pazos, R., Royo, F., González, E., Roura-Ferrer, M., Martínez, A., Gamiz, J., Reichardt, N. C., & Falcón-Pérez, J. M. (2019). Assessing the role of surface glycans of extracellular vesicles on cellular uptake. *Scientific Reports*, 9, 1–14. <https://doi.org/10.1038/s41598-019-48499-1>
- Wu, C. H., Li, J., Li, L., Sun, J., Fabbri, M., Wayne, A. S., Seeger, R. C., & Jong, A. Y. (2019). Extracellular vesicles derived from natural killer cells use multiple cytotoxic proteins and killing mechanisms to target cancer cells. *Journal of Extracellular Vesicles*, 8. <https://doi.org/10.1080/20013078.2019.1588538>

SUPPORTING INFORMATION

Additional supporting information can be found online in the Supporting Information section at the end of this article.

How to cite this article: Zheng, W., He, R., Liang, X., Roudi, S., Bost, J., Coly, P.-M., van Niel, G., & Andaloussi, S. E. L. (2022). Cell-specific targeting of extracellular vesicles through engineering the glycocalyx. *Journal of Extracellular Vesicles*, 11, e12290. <https://doi.org/10.1002/jev2.12290>